Astronomy & Astrophysics

The influence of redshift information on galaxy-galaxy lensing measurements

M. Kleinheinrich[1,2], H.-W. Rix[1], T. Erben[2], P. Schneider[2], C. Wolf[3], M. Schirmer[2], K. Meisenheimer[1], A. Borch[1], S. Dye[4], Z. Kovacs[1], and L. Wisotzki[5]

[1] Max-Planck-Institut für Astronomie, Königstuhl 17, 69117 Heidelberg, Germany
    e-mail: martina@mpia.de
[2] Institut für Astrophysik und Extraterrestrische Forschung, Universität Bonn, Auf dem Hügel 71, 53121 Bonn, Germany
[3] Department of Physics, Denys Wilkinson Bldg., University of Oxford, Keble Road, Oxford OX1 3RH, UK
[4] School of Physics and Astronomy, Cardiff University, 5 The Parade, Cardiff CF24 3YB, UK
[5] Astrophysikalisches Institut Potsdam, An der Sternwarte 16, 14482 Potsdam, Germany

Abstract. We investigate how galaxy-galaxy lensing measurements depend on the knowledge of redshifts for lens and source galaxies. Galaxy-galaxy lensing allows one to study dark matter halos of galaxies statistically using weak gravitational lensing. Redshift information is required to reliably distinguish foreground lens galaxies from background source galaxies and to convert the measured shear into constraints on the lens model. Without spectroscopy or multi-colour information, redshifts can be drawn from independently estimated probability distributions. The COMBO-17 survey provides redshifts for both lens and source galaxies. It thus offers the unique possibility to do this investigation with observational data. We find that it is of great importance to know the redshifts of individual lens galaxies in order to constrain the properties of their dark matter halos. Whether the redshifts are derived from *UBVRI* or the larger number of filters available in COMBO-17 is not very important. In contrast, knowledge of individual source redshifts improves the measurements only very little over the use of statistical source redshift distributions as long as the source redshift distribution is known accurately.

Key words. gravitational lensing – methods: data analysis – galaxies: fundamental parameters – galaxies: statistics – cosmology: dark matter

1. Introduction

Weak gravitational lensing of galaxies by galaxies (galaxy-galaxy lensing) provides a unique tool to study the dark matter distribution in lens galaxies. A foreground galaxy distorts the images of background galaxies such that they are, on average, tangentially aligned with respect to the lens. This alignment can be measured statistically, see e.g. Mellier (1999); Bartelmann & Schneider (2001) for reviews.

In the beginning, galaxy-galaxy lensing was measured from imaging data alone without any direct redshift information (e.g. Brainerd et al. 1996; dell'Antonio & Tyson 1996; Fischer et al. 2000). However, multi-colour or spectroscopic data are desirable for two reasons:

1. The strength of the gravitational shear and thus the image distortion depends on the angular diameter distances between observer, lens and source. In turn, redshift estimates for the lens and source galaxies are therefore needed to translate the measured distortion reliably into constraints on the lens galaxies.
2. The need for averaging over at least hundreds of lens galaxies complicates the interpretation of the results severely

unless physically similar subsets of galaxies can be identified. As the luminous parts of galaxies cover a large range of properties, it is clear that galaxies also differ in the properties of their dark matter halos (e.g. McKay et al. 2002; Prada et al. 2003). To learn something about different galaxy types one needs to be able to classify the potential lens galaxies at least by their luminosities and rest-frame colours, which requires redshift estimates. Note, that for this application the redshift precision required is only a few percent, not the 10^{-4} of spectroscopic surveys.

Redshifts and/or classification for the lens galaxies have been used by several authors now (e.g. Smith et al. 2001; Wilson et al. 2001; McKay et al. 2001; Guzik & Seljak 2002; Hoekstra et al. 2003), while redshifts for the source galaxies have so far only been used by Hudson et al. (1998) who measured galaxy-galaxy lensing in the Hubble Deep Field North, and more recently by Sheldon et al. (2004) using the Sloan Digital Sky Survey (SDSS). All other studies used redshift probability distributions at a given apparent magnitude to assign redshifts to the source and – where necessary – to the lens galaxies. These probability distributions have been derived from galaxy redshift surveys like the Canada-France Redshift Survey

(Crampton et al. 1995) or the Caltech Faint Galaxy Redshift Survey (Cohen et al. 2000). However, for the deeper data sets, the measured redshift probability distributions had to be extrapolated to the fainter magnitudes of the source galaxies.

In this paper we address the question of how measurements of dark matter halos with galaxy-galaxy lensing are affected by incomplete redshift information. We use observational data with accurate photometric redshifts for both lens and source galaxies. We perform the measurements with (a) the full information for lens and source galaxies, (b) full information for the lens galaxies but drawing the redshifts of the sources from probability distributions, and (c) using probability distributions to estimate redshifts for lenses and sources. Although in case (a) we use the full redshift information, this measurement is not an optimal measurement of galaxy-galaxy lensing from COMBO-17. In this paper, the lens and source selection is always based on apparent magnitudes and angular separations which allows us to compare the results from the different cases. However, for retrieving the tightest and most meaningful constraints on the dark matter halos of galaxies, one should clearly use redshifts also for the lens and source selection. This will be done in a companion paper (Kleinheinrich et al. 2004).

In Sect. 2 we describe the data set followed by an overview of our method of measuring galaxy-galaxy lensing in Sect. 3. Section 4 explains how we estimate redshifts and luminosities. In Sect. 5 we present our measurements and results. We close with a summary in Sect. 6.

2. Data

We use the COMBO-17 survey for our lensing analysis. Properties of the galaxy sample have already been described in Wolf et al. (2003). A more detailed and updated description of the final catalogs used here is given in Wolf et al. (2004). COMBO-17 has already been applied to various weak lensing studies including detailed analysis of the supercluster Abell 901/902 (Gray et al. 2002, 2004; Taylor et al. 2004) and cosmic shear (Brown et al. 2003; Bacon et al. 2004).

COMBO-17 is a deep optical survey carried out with the Wide Field Imager (WFI) at the MPG/ESO 2.2-m telescope on La Silla, Chile. It consists of four fields covering about 0.26 square degrees each and has in its deepest stacked R-band image a 5-σ point source limit of $R \sim 26$. Observations in $UBVRI$ and 12 optical medium-band filters yield spectral classification and photometric redshifts with $\sigma_z/(1 + z) < 0.01$ for $R < 21$, and deteriorating to $\sigma_z/(1 + z) \approx 0.05$ for $R \approx 24$. The R-band observations were carried out in the best seeing conditions (typically $0\rlap{.}''75$) enabling accurate shape measurements for weak lensing studies. Currently, the data set is fully processed for three survey fields (see Wolf et al. 2003), which will all be used here. Although in principle all data needed for our analysis is available from the standard COMBO-17 data reduction, we only use those data for measurements based on photometry. This includes apparent magnitudes, redshift estimates, classification and the derivation of rest-frame luminosities. The data reduction pipeline of COMBO-17 is optimized for photometric measurements, but it creates only simple sum images for object detection and crude shape measurements.

In particular, the sum images in COMBO-17 were created using only full pixel shifts when stacking individual exposures. Therefore, they are not optimal for shape measurements. Instead, we detect objects and measure their shapes from coadded R-band images created with the data reduction pipeline of the Garching-Bonn Deep Survey (GaBoDS, Schirmer et al. 2003). In the coaddition of the image on the CDFS field we included observations from the ESO Imaging Survey and from GOODS. The exposure times and the seeing are 57 000 s and $0\rlap{.}''88$ for the CDFS field, 21 600 s and $0\rlap{.}''88$ for the S 11 field, and 24 900 s and $0\rlap{.}''74$ for the A 901 field. From these summed images we measure positions, shapes and half-light radii.

Note that the summed images used here are not identical to those used in previous COMBO-17 lensing studies listed above. Also, application of the KSB algorithm for shape measurement differs slightly (see Sect. 2.1). A joint effort to compare the results from the different analyses is currently underway (Heymans et al. in prep.).

The original field selection in COMBO-17 was not random. The A 901 field was chosen because of the presence of a supercluster composed of Abell 901a,b and Abell 902 at $z = 0.16$. Conversely, the CDFS field was originally chosen because of its emptiness. The S 11 field is the only random field. In Kleinheinrich et al. (2004) we will present a detailed analysis showing that the clusters in the A 901 field do not affect the galaxy-galaxy lensing measurement. Therefore, in this paper we completely ignore the presence of these clusters.

2.1. Shape measurements

The coaddition of individual images into deep summed frames with the GaBoDS pipeline (*THELI*) is described in detail in Schirmer et al. (2003). This pipeline was specifically developed for data from multichip cameras such as the WFI with 2×4 chips. The stacked images cover the whole CCD mosaic unlike having stacked images for each individual chip. However, due to e.g. different sensitivities of the CCDs and gaps between them, the exposure times and noise properties vary across the stacked images. Therefore, an additional weight image is created that keeps track of these varying noise properties. The object catalog is obtained by running SExtractor (Bertin & Arnouts 1996) on the stacked images using the weight images. The use of the weight images very efficiently suppresses spurious source detections. We therefore do not apply further masking of objects by hand.

For the detected objects we use the KSB algorithm (Kaiser et al. 1995; Luppino & Kaiser 1997; Hoekstra et al. 2000) to measure shapes and correct these for the point spread function (PSF). For such a correction we use the shapes of stellar objects to trace the shape and variation of the PSF across the image; see also Bartelmann & Schneider (2001) for a summarizing description of the KSB algorithm and Erben et al. (2001) for details of its application as used here.

Ellipticities are calculated from weighted second order-moments Q_{ij} of the light distribution $I(x)$

$$Q_{ij} = \int d^2x W(x) x_i x_j I(x). \tag{1}$$

Here, x denotes the position (a vector in the complex plane) with respect to the object center, $W(x)$ is a weight function and $f(x)$ the flux at position x. For the weight function $W(x)$ we use a Gaussian filter function with the half-light radius θ_h of the object under consideration (determined by SExtractor) as the window scale. A complex ellipticity $\chi = \chi_1 + i\chi_2$ is defined as

$$\chi_1 = \frac{Q_{11} - Q_{22}}{Q_{11} + Q_{22}}, \quad \chi_2 = \frac{2Q_{12}}{Q_{11} + Q_{22}}. \tag{2}$$

The correction, q, for the spatially varying anisotropic part of the PSF is applied by fitting a fourth-order polynomial to the ellipticities of stellar objects across the whole field-of-view.

The subsequent correction for the isotropic part of the PSF is done as a function of galaxy size. This means that the shear polarizability P^{sh} and the smear polarizability P^{sm} of stellar objects are measured with a range of window scales. For each object, the measurement from the window scale matching θ_h of that object is used in the correction. P^{sh} and P^{sm} are tensors that describe, for a given weight function W, the response of the measured ellipticities to gravitational shear in the absence of PSF effects (P^{sh}) and to the isoptropic smearing by the PSF (P^{sm}). P^{sh} and P^{sm} are measured from the third and fourth-order moments of the light distribution of an object. An estimator of the shear is then given by

$$\epsilon = (P^g)^{-1}\chi_{aniso} \tag{3}$$

with

$$P^g = P^{sh} - P^{sm}(P^{*sm})^{-1}P^{*sh}. \tag{4}$$

The quantities with asterisks are measured from the stellar objects only, and $\chi_{aniso} = \chi + P^{sm}q^*$ is the anisotropy-corrected ellipticity. Instead of using full tensors in Eqs. (3) and (4) we apply the scalar correction by only using the trace of P^g. Furthermore, we use raw values of P^g although this leads in some cases to unphysically large PSF-corrected ellipticities ($\epsilon > 1$) due to noise. However, Erben et al. (2001) found that fitting P^g does not improve the shape measurement. We use the weighting scheme proposed by Erben et al. (2001) to downweight objects with noisy ellipticity estimates. This procedure will be explained in more detail in Sect. 3.

3. Method

For extracting the galaxy-galaxy lensing signal from a set of measured galaxy ellipticities and, potentially, redshifts, we use the maximum-likelihood method by Schneider & Rix (1997). We parametrize the lens galaxies as singular isothermal spheres

$$\rho(r) = \frac{\sigma_v^2}{2\pi G} \frac{1}{r^2}, \tag{5}$$

where σ_v is the velocity dispersion of a galaxy. Furthermore, we assume that the velocity dispersion scales with luminosity as

$$\frac{\sigma_v}{\sigma_*} = \left(\frac{L}{L_*}\right)^\eta, \tag{6}$$

where σ_* is the velocity dispersion of an L_* galaxy. We adopt $L_* = 10^{10} L_\odot$, measured in the SDSS r-band. For each lens-source pair the shear is given by

$$\gamma(r) = \frac{2\pi\sigma_v^2}{c^2} \frac{D_{ds}}{D_s} \frac{1}{\theta}, \tag{7}$$

where D_s is the angular diameter distance between the observer and source, and D_{ds} is that between the lens and source, while θ is the angular separation between lens and source. For the calculation of angular diameter distances from the galaxy redshifts, we adopt $(\Omega_m, \Omega_\Lambda) = (0.3, 0.7)$ and $H_0 = 100h$ km s^{-1}Mpc^{-1}.

Following Schneider & Rix (1997), for each source galaxy j the total shear γ_j from all lenses lying within a certain annulus around the source is calculated for a range of trial input parameters (σ_*, η). The resolution of our grid in parameter space is $\Delta\sigma_\star = 6$ km s^{-1} and $\Delta\eta = 0.03$. From γ_j and the observed ellipticity ϵ_j the intrinsic ellipticity

$$\epsilon_j^{(s)} = \epsilon_j - \gamma_j \tag{8}$$

is estimated. The probability for observing this intrinsic ellipticity is given by

$$P(\epsilon_j^{(s)}) = \frac{1}{\pi\sigma_\epsilon^2} \exp\left[-\frac{|\epsilon_j^{(s)}|^2}{\sigma_\epsilon^2}\right], \tag{9}$$

where σ_ϵ is the width of the intrinsic ellipticity distribution. Multiplying the probabilities $P(\epsilon_j^{(s)})$ from all sources gives the likelihood for a given set of (σ_*, η) which is then maximized to find the best-fit parameters.

The value of σ_ϵ can be estimated from the data set itself. However, we find that the average ellipticity depends systematically on, e.g., the signal-to-noise S/N or on the half-light radius θ_h of the objects. This behaviour was suggested by the weighting scheme proposed by Erben et al. (2001) who assumed that the noise properties of objects are traced by these quantities. They then suggest the inverse of the variance $\sigma_\epsilon^2 = \frac{1}{N}\sum|\epsilon|^2$ as the weight of an object j in the ellipticity estimates of the $N \approx 20$ objects being closest to object j in $\theta_h - $ S/N space. We use σ_ϵ from this weighting scheme with $N = 20$ as an estimate of the width of the intrinsic ellipticity distribution for each object j. This choice of σ_ϵ directly accounts for errors in the shape measurement but also for intrinsic changes of σ_ϵ with half-light radius and S/N which might be due to changes in the galaxy population. Typical values are $\sigma_\epsilon \approx 0.4$.

The method of Schneider & Rix (1997) described so far only works if the lens and source galaxy redshifts are known. If that is not the case, one can calculate the shear γ by integrating over a given redshift probability distribution which must be done numerically. We use Monte Carlo integration and assign random redshifts to the galaxies 50 times, see Schneider & Rix (1997). The redshift probability distribution used is described in Sect. 4.

4. Redshift distribution

For many of the COMBO-17 galaxies we have fairly precise redshifts. However, for the majority of sources, with $R > 23.5$, and for other data sets, we have not. Therefore, we briefly describe how to create Monte Carlo redshifts, given an apparent galaxy magnitude.

A parametrization of a redshift probability distribution which has often been used in weak lensing is given by (Baugh & Efstathiou 1993)

$$\frac{dN}{dz} \propto \frac{z^2}{z_\star^3} \exp\left[-\left(\frac{z}{z_\star}\right)^{1.5}\right].\tag{10}$$

$z_\star$ is related to the median redshift z_m of the distribution by

$$z_\star = z_m/1.412.\tag{11}$$

Brown et al. (2003) calculated median redshifts z_m for different bins in magnitude and found that in COMBO-17 z_m increases with median R-band magnitude as

$$z_m = 2.53162 - 0.329974 \times R + 0.0108296 \times R^2.\tag{12}$$

For each object we assign a random redshift by first calculating z_m from its R-band magnitude and using this z_m in Eqs. (10) and (11).

When we estimate the redshifts of the lens galaxies we also have to estimate their luminosities. We use

$$L = \left(\frac{H_0 D_d}{c}\right)^2 (1 + z)^6 10^{0.4(21.4 - R)}\tag{13}$$

to relate the luminosity of a galaxy in units of L_* to its apparent R-band magnitude and redshift z (Brainerd et al. 1996). The exponent of the $1 + z$ term includes an estimate of the k-correction. We compared the luminosities calculated from our measured redshifts and Eq. (13) to those derived directly in COMBO-17, in order to test the accuracy of Eq. (13) and to determine its normalization. For 62% of the galaxies the luminosity estimate differs by less than 20% from that measured within COMBO-17.

5. Measurements and results

For all measurements we constrain lenses to have magnitudes $R = 18-22$ and sources to $R = 22.5-24$. Additionally, we require sources to have a half-light radius larger than the PSF of the corresponding summed frame. The maximum projected distance at which we still consider a lens acting on a source is $35''$, corresponding to an impact parameter of about $130h^{-1}$ kpc for a typical lens redshift $z = 0.4$. We find that inclusion of pairs with larger projected distances reduces the significance of our measurements. Furthermore, we exclude all pairs which are closer than $8''$ because there the shape measurement of the source may be affected by the light from the lens. Note that the average half-light radius of the lens population is $0\rlap{.}''85$ with a maximum of about $3.5''$. Only objects identified as galaxies in the multi-colour classification are used as lenses. Therefore, unresolved galaxies are included in the lens sample.

Table 1. Numbers of lenses N_d, sources N_s and pairs N_p used in the different measurements. For (b) and (c) N_p is only the number of pairs averaged over the different MC realizations, while N_d and N_s give the number of lenses and sources that are used in any of the MC realizations. The last two columns give the best fit values of σ_* and η with 1-σ error bars marginalized over the other variable.

case	N_d	N_s	N_p	σ_* [km s^{-1}]	η
(a)	7629	13 026	38 785	150^{+24}_{-18}	$0.22^{+0.09}_{-0.09}$
(b)	7629	18 563	50 521	144^{+18}_{-24}	$0.22^{+0.12}_{-0.12}$
(c)	7629	18 563	49 764	156^{+24}_{-30}	$0.49^{+0.15}_{-0.21}$

Three main cases differing in sample size and extent of redshift information are used to investigate the influence of redshift information on the likelihood contours for the parameters (σ_*, η):

(a) Lens and source candidates must be classified as galaxies and have a redshift measurement; redshifts from COMBO-17 are used for lenses and sources.

(b) The lens sample is the same as in case (a) but sources can be all resolved objects within the required magnitude range. Redshifts from COMBO-17 are used for lenses whereas the redshifts of sources are drawn from probability distributions based on their magnitudes.

(c) Lens and source sample are the same as in case (b) but redshifts from COMBO-17 are not used at all. Lenses and sources are assigned random redshifts based on their apparent magnitudes and using Eqs. (10)–(12). Then, the luminosities of the lenses are estimated from apparent magnitudes using Eq. (13).

In all cases we use the same lens sample. Therefore, any differences in the parameter estimates must be due to either the accuracy of the redshifts or to a change in the source sample. Note that we cannot straightforwardly use the same source sample in all three cases as we do with the lens sample. This is because the redshift probability distribution described in Sect. 4 was derived taking the completeness of the COMBO-17 redshifts into account, see also Sect. 5.1.1.

Table 1 gives the number of lenses, sources and pairs used in each measurement and the best-fit (σ_*, η) values with their 1-σ uncertainties. The corresponding likelihood contours are shown in Fig. 1.

5.1. The role of individual source redshifts

Compared to case (a), individual redshifts for the source galaxies are omitted in case (b) and replaced by redshifts drawn from a probability distribution. Additionally, objects without COMBO-17 redshifts are included in the source sample and increase it by about 40%.

Table 1 and Fig. 1 show no significant change in the best-fit parameters and the 1-σ error bars. Recall that a difference of 6 km s^{-1} in $\sigma_\star$ and 0.03 in η is just the resolution of our grid in parameter space. Figure 1 further shows a widening of the 2- and 3-σ likelihood contours together with an extension towards low $\sigma_\star$ and low η. The comparison of cases (a)
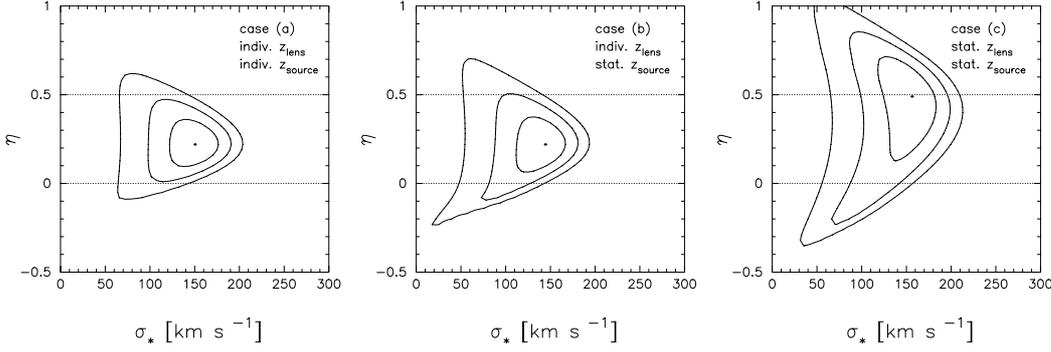
Fig. 1. Likelihood contours for the lens model described in Sect. 3, contours are 1-, 2- and 3-σ. *Left panel*: redshift information is used for lens and source galaxies, *middle panel*: redshift information is only used for lenses, *right panel*: redshift information is not used at all.

and (b) shows that the tightest constraints are obtained from using only sources with measured redshift although this implies that potential sources are ignored. However, the use of redshift probability distributions instead of individual redshifts for the sources still leads to almost as good constraints.

The next subsections give some more tests on the influence of source redshifts on the galaxy-galaxy lensing measurement.

5.1.1. Source sample from case (a) but with statistical redshifts

The derivation of the redshift probability distribution in Sect. 4 takes the magnitude- and redshift-dependent completeness of the redshifts in COMBO-17 into account (see Wolf et al. 2004, Fig. 14). For the magnitudes of the lens sample, the completeness reaches 100% at all redshifts. For the fainter magnitudes of the sources, however, the completeness is a function of redshift. Here, the completeness is largest for $z \approx 1$ and declines toward lower and higher redshift. Therefore, the redshift distribution of all sources with COMBO-17 redshift does not follow the probability distribution given in Eqs. (10)–(12) and we can thus not use the same source sample as in case (a) and assign random redshifts from Eqs. (10)–(12). Indeed, when trying this we obtained a best-fit $\sigma_\star$ that was 1-σ above the best-fit from case (a).

5.1.2. Statistical redshifts only for sources without COMBO-17 redshift

We use the same source selection here as in case (b). The difference is that here COMBO-17 redshifts are used whenever they are available for a source. Only those sources without COMBO-17 redshift are assigned a random redshift. The best-fit parameters remain unchanged compared to case (b) but the likelihood contours become tighter than in case (b). The upper limits (1−3σ) on $\sigma_\star$ remain almost unchanged, but the lower limits increase. The 3-σ lower limit is increased from 36 km s^{-1} in case (b) to 60 km s^{-1} here. On the other hand, the contours are still slightly wider than in case (a). This leads to two conclusions: (1) the comparison of cases (a) and (b) shows that knowledge of individual source redshifts only slightly

improves the constraints by excluding very small values of the velocity dispersion; (2) the comparison with case (a) also shows that the inclusion of additional sources without COMBO-17 redshift does not improve but rather weakens the constraints. This result appears, at first sight, somewhat surprising, yet can probably be explained by the fact that objects without COMBO-17 redshifts are mainly faint. But faint objects have less accurate and useful shape measurements than brighter ones and therefore hardly influence the constraints.

Strictly speaking we should not apply the redshift distribution from Sect. 4 to the sample of sources without COMBO-17 redshifts for the reasons detailed in Sect. 5.1.1. However, these account for only about 30% of all sources used in this case. Furthermore, they seem to have too noisy shape measurements, and thus little weight, so that the slightly wrong redshift probability distribution does not play a significant role.

5.1.3. Median instead of random redshifts

Given the small influence individual source redshifts seem to have we explored how the results would change if we do not use Monte Carlo integration to deal with the redshift probability distribution. Instead, we assign each source of case (b) a fixed redshift which is just the median redshift at the magnitude of the source, see Eq. (12). The advantage is that then the computation is simplified and becomes much faster than requiring 50 Monte Carlo realizations. Compared to case (b) we find a small shift of the likelihood contours towards higher η. The shift is 1−2 gridpoints, so $\Delta\eta = 0.03$−0.06. In the direction of $\sigma_\star$ we do not see any change.

5.1.4. Sensitivity to changes in the redshift probability distribution

Instead of the redshift distribution derived from the COMBO-17 data itself we now test the redshift probability distribution given by Brainerd et al. (1996). This probability distribution assumes a linear relation between magnitude and redshift. At $R = 24$ it predicts a roughly 20% smaller redshift than our model, yielding only a 10% change in the angular diameter distance in our cosmology. At fixed

lens redshift z_d, the ratio D_{ds}/D_s also becomes smaller with decreasing source redshift z_s. Equation (7) shows that underestimating the source redshift will overestimate the velocity dispersion $\sigma_\star$. Indeed we measure, using the same sources as in case (b), a larger best-fit $\sigma_\star = 156$ km s^{-1} when using the redshift probability distribution from Brainerd et al. (1996), compared to $\sigma_\star = 144$ km s^{-1} for case (b). This shift is not significant given the large error bars of our measurement of galaxy-galaxy lensing. However, it might be significant for larger surveys with better statistics like the Sloan Digital Sky Survey (e.g. Guzik & Seljak 2002) or the Red Sequence Cluster Survey (e.g. Hoekstra et al. 2004).

5.2. Importance of individual lens redshifts

Going from case (b) to (c), individual redshifts for the lenses are omitted as well and replaced by redshifts drawn from a probability distribution. Consequently, the luminosity measurement from COMBO-17 is replaced by luminosities estimated from apparent magnitudes and redshifts as described in Sect. 4.

Table 1 and Fig. 1 show a dramatic change in the likelihood contours. The best-fit velocity dispersion increases from $\sigma_\star = 144$ km s^{-1} to $\sigma_\star = 156$ km s^{-1} and the 1-σ error increases by about 30%. The shift towards higher velocity dispersion is not significant. The best-fit η, on the other hand, becomes significantly larger (2-σ significance) and the 1−3σ errors increase by about 50−100%.

As for the sources, we perform some tests on the influence of lens redshifts on the galaxy-galaxy lensing measurement.

5.2.1. Influence of the luminosity estimation

First, we investigate whether there is any difference between using the luminosities derived from COMBO-17 photometry and the luminosities estimated using Eq. (13) with the correct redshift and apparent magnitude of a lens; this assumption enters only in Eq. (6). Surprisingly, the likelihood contours remain almost unchanged and also the best-fit values just change by $\Delta\eta = 0.03$ towards smaller η. It seems that the luminosities of the lenses do not have to be known very accurately.

5.2.2. Influence of lenses with too low redshift estimate

When using random redshifts for the lenses in case (c), the redshifts of some lens candidates will be underestimated so that these galaxies are considered as lenses although they lie behind the actual source. Here, we exclude all such pairs, that is, we perform a measurement as in case (c) but use only those lens-source pairs for which the COMBO-17 redshift of the lenses is lower than the redshift estimate of the sources. This reduces the number of pairs from 49 764 to 44 738 while the number of lenses and sources remains the same as in case (c). The best-fit parameters become $\sigma_\star = 156^{+24}_{-24}$ km s^{-1} and $\eta = 0.49^{+0.15}_{-0.24}$. The contours become slightly tighter than in case (c) but there is no big change.

5.2.3. Influence of non-galaxy lenses

So far, in all our measurements we used the same set of lenses. In particular, these are only objects which are classified as galaxies or likely galaxies. However, in the absence of individual redshifts, typically no such classification is available. Therefore, we here use all objects with $R = 18−22$ as lenses regardless of their classification by COMBO-17. Furthermore, we exclude all unresolved objects from the lens sample. The new lens sample contains 7719 objects, of which 7405 were already used in cases (a)−(c). 224 lenses from cases (a)−(c) are excluded here because they are unresolved. On the other hand, 314 lenses are used here but were not considered in cases (a)−(c). Of these, 217 are classified as galaxies and have redshift estimates so that they could in principle have been used as lenses. These 217 galaxies did not enter the lens sample of case (a) because they have no source from case (a) within 35″. The remaining 97 lenses that are used here but not in cases (a)−(c) are 28 stars, 30 quasars, 4 strange objects and 35 galaxies without redshift estimates. Therefore, the contamination of our lens sample here from non-galaxy objects is below 1%. The likelihood contours shift towards smaller $\sigma_\star$ and larger η compared to case (c) and the contours become wider. The best-fit parameters become $\sigma_\star = 144^{+24}_{-30}$ km s^{-1} and $\eta = 0.52^{+0.18}_{-0.21}$. When leaving out the 62 non-galaxy lenses the likelihood contours remain essentially the same. This shows that the shift of the likelihood contours compared to case (c) is not due to the inclusion of non-galaxy objects but to a change in galaxy population of the lens sample.

5.2.4. COMBO-17 redshifts with COMBO-17 errors

To explore how precise individual lens redshift measurements should be, we use the redshift errors from COMBO-17 to assign random redshifts with increasing errors to the lenses. Galaxies in the magnitude range $R = 18−22$ have redshift errors $\sigma_z \leq 0.223$ with a mean of about $\langle\sigma_z\rangle \approx 0.02$. Random redshifts are assigned to each lens with redshift z and redshift error σ_z using a Gaussian distribution with mean z and width $f \times \sigma_z$. Even for $f = 10$ the likelihood contours are only slightly wider than those in case (b). It is therefore apparent that the error on the lens redshifts can become fairly large without changing the results significantly. However, by design, each lens gets on average the correct redshift assigned so that this statement only holds true for unbiased estimates of the mean.

5.2.5. Redshifts from *UBVRI* only

Finally, we investigate a case intermediate between case (b) where full redshift information for the lenses is available, and case (c) without any redshift information. We assign redshifts to the sources as in case (b) while for the lenses we use redshifts derived from only the 5 broad-band filters *UBVRI*. The redshifts are estimated using exactly the same technique as for 17 filters.

First, we briefly summarize the differences between the redshifts and classification from 5 and 17 filters for potential
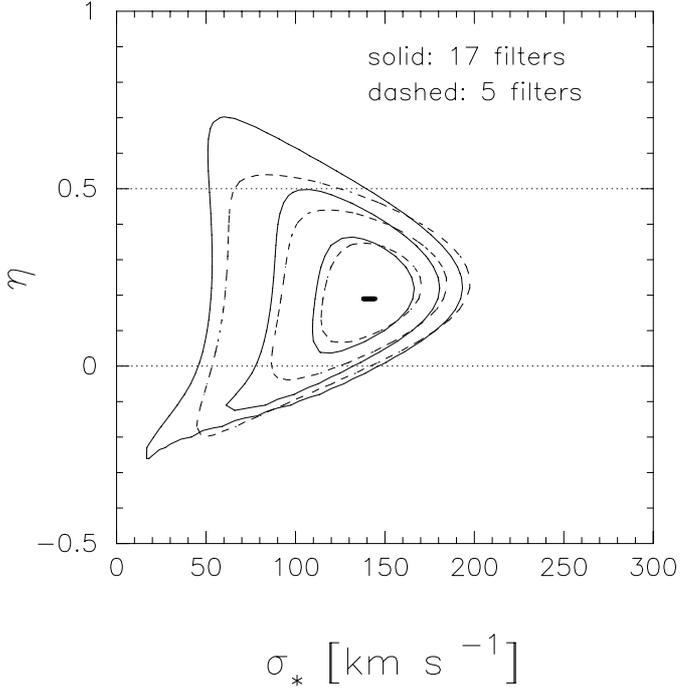
Fig. 2. Likelihood contours for the lens model described in Sect. 3, contours are 1-, 2- and 3-σ. Solid lines correspond to a measurement where all 17 filters are used for redshift estimation and classification, dashed contours show the same with redshift estimation and classification based on just five broad-band filters.

lenses, i.e. objects with $R = 18-22$. From the 10 908 objects in that magnitude range 8124 objects are classified (on the basis of their SED) as galaxies both times. Only 21 objects are classified as galaxies in the 17-filter classification but missed in the 5-filter classification. From just broad-band filters these 21 objects are mainly classified as quasars (15 objects). Conversely, 733 objects are classified as galaxies from the broad-band filters although with 17 filters they are identified as mainly stars (697 objects) but also quasars (32 objects) or strange objects (4 objects). The redshift difference for objects classified as galaxies both times is on average only $\langle z_5 - z_{17} \rangle = -0.017 \pm 0.074$, where the subscript indicates the number of filters used for the redshift estimation. The difference in the SDSS r-band restframe magnitude M_r is on average 0.12 ± 0.67 mag implying that on average the luminosities are 10% smaller when derived from 5 filters. However, the scatter is very large so that the luminosity estimates can differ by great factors for individual objects. The typical magnitude difference is $\sqrt{\langle (M_{r,5} - M_{r,17})^2 \rangle} = 0.68$. This implies that the luminosities are typically wrong by almost a factor of 2! The cause of this are different and less accurate redshift values that the classification based on five filters gives for each galaxy compared to the 17-filter classification. As a result not only the luminosity distances but also the K corrections change, since we place our restframe band into a slightly different part of the observed-frame SED. Both effects together lead to a less accurate luminosity estimate.

Figure 2 shows likelihood contours obtained from the 17-filter classification and from the 5-filter classification with

the same set of 7577 lens and 18 553 source galaxies being used. In both cases, the redshifts of the sources are estimated from their magnitudes as in case (b). The best-fit parameters with 1-σ errors are $\sigma_\star = 144^{+18}_{-24}$ km s^{-1} and $\eta = 0.19^{+0.12}_{-0.12}$ for the 17-filter classification and $\sigma_\star = 144^{+24}_{-24}$ km s^{-1} and $\eta = 0.19^{+0.12}_{-0.09}$ for the 5-filter classification. The agreement between the two measurements is very good. Surprisingly, the constraints on η are even tighter from the 5-filter classification than when using the full COMBO-17 filterset. The differences appear just for large values of η. However, the upper bound of η is determined from the brightest lenses which would be weighted highly (from Eq. (6)) for large η. Therefore, excluding the brightest lenses does increase the upper bound on η. Although, on average, luminosities are underestimated in the 5-filter classification, we see exactly the opposite for bright objects. For example, 235 objects have $L > 5L_\star$ in the 5-filter classification. On average, these 235 objects are 0.29 mag brighter than in the 17-filter classification so that their luminosities are overestimated by about 30%. For the 60 objects with $L > 10L_\star$ this difference becomes 1.16 mag or a factor of almost 3 in luminosity. Therefore, we think that the tighter contours derived from the 5-filter classification do not mean that better constraints can be obtained but rather shows the limitations of this smaller filter set compared to the whole 17-filter classification.

Finally, we use all lenses from the 5-filter classification including those which were not classified as galaxies from the full 17-filter set. Compared to the 5-filter case in Fig. 2 the contours change only weakly (at most 1 gridpoint) towards smaller $\sigma_\star = 138^{+18}_{-24}$ km s^{-1} and $\eta = 0.19^{+0.09}_{-0.12}$. This shows again that 10% false lenses in the sample do not effect our results severely.

6. Summary and outlook

We used the COMBO-17 survey to investigate the importance of individual redshift measurements on galaxy-galaxy lensing studies. We find that redshift information for the lens galaxies plays a crucial role in constraining their dark matter halos while for the source galaxies it is sufficient to have roughly correct redshift probability distributions available. We have also seen that redshifts obtained from just $UBVRI$ ($\langle \sigma_z/(1 + z) \rangle = 0.03$ for $R = 18-22$) instead of the full 17 filter set available in COMBO-17 ($\langle \sigma_z/(1 + z) \rangle = 0.015$ for $R = 18-22$) are sufficient to constrain the redshifts of the lenses and their rest-frame luminosities.

However, some benefits from the 17-filter classification remain. Most importantly, the 17-filter classification was used to derive the redshift probability distribution of the source population. In deep weak lensing studies, sources are typically fainter than the magnitude limit of current galaxy redshift surveys. Therefore, any redshift probability distribution can only be obtained from extrapolation to faint magnitudes. In Sect. 5.1.4 we have shown that this extrapolation can introduce a bias into the measurement that is of the same order or even larger than the errors from large surveys like the RCS or SDSS. In principle, the redshift distribution of the sources could also be derived from just 5 filters. However, from 5 filters, the decrease

in redshift accuracy is larger for the fainter sources than for the brighter lenses. Furthermore, fewer sources get reliable redshift estimates from 5 than from 17 filters. Therefore, the source redshift distribution derived from 5 filters will be less accurate than from 17 filters.

The gain from multi-colour or spectroscopic data for the lenses will even be larger than shown from the comparisons in this paper. Knowledge of individual redshifts will allow one to select lenses and sources not from less reliable magnitude cuts but from the redshifts themselves. Redshifts will also allow one to include fainter lenses or, when redshifts are available for the sources as well, brighter sources and will thus improve the statistics.

Any information on the nature of the lens galaxies will additionally allow one to investigate if and how the properties of the dark matter halos depend on galaxy classes which can be defined according to e.g. luminosity, colour, stellar mass or environment. Such investigations are necessary to test and improve our understanding of galaxy formation and evolution where dark matter is supposed to play a major role.

References

Bacon, D. J., Taylor, A. N., Brown, M. L., et al. 2004, MNRAS, submitted [arXiv:astro-ph/0403384]

Bartelmann, M., & Schneider, P. 2001, Phys. Rep., 340, 291

Baugh, C. M., & Efstathiou, G. 1993, MNRAS, 265, 145

Bertin, E., & Arnouts, S. 1996, A&AS, 117, 393

Brainerd, T. G., Blandford, R. D., & Smail, I. 1996, ApJ, 466, 623

Brown, M. L., Taylor, A. N., Bacon, D. J., et al. 2003, MNRAS, 341, 100

Cohen, J. G., Hogg, D. W., Blandford, R., et al. 2000, ApJ, 538, 29

Crampton, D., Le Fevre, O., Lilly, S. J., & Hammer, F. 1995, ApJ, 455, 96

dell'Antonio, I. P., & Tyson, J. A. 1996, ApJ, 473, L17

Erben, T., Van Waerbeke, L., Bertin, E., Mellier, Y., & Schneider, P. 2001, A&A, 366, 717

Fischer, P., McKay, T. A., Sheldon, E., et al. 2000, AJ, 120, 1198

Gray, M. E., Taylor, A. N., Meisenheimer, K., et al. 2002, ApJ, 568, 141

Gray, M. E., Wolf, C., Meisenheimer, K., et al. 2004, MNRAS, 347, L73

Guzik, J., & Seljak, U. 2002, MNRAS, 335, 311

Hoekstra, H., Franx, M., & Kuijken, K. 2000, ApJ, 532, 88

Hoekstra, H., Franx, M., Kuijken, K., Carlberg, R. G., & Yee, H. K. C. 2003, MNRAS, 340, 609

Hoekstra, H., Yee, H. K. C., & Gladders, M. D. 2004, ApJ, 606, 67

Hudson, M. J., Gwyn, S. D. J., Dahle, H., & Kaiser, N. 1998, ApJ, 503, 531

Kaiser, N., Squires, G., & Broadhurst, T. 1995, ApJ, 449, 460

Kleinheinrich, M., Schneider, P., Rix, H. W., et al. 2004 [arXiv:astro-ph/0412615]

Luppino, G. A., & Kaiser, N. 1997, ApJ, 475, 20

McKay, T. A., Sheldon, E. S., Racusin, J., et al. 2001 [arXiv:astro-ph/0108013]

McKay, T. A., Sheldon, E. S., Johnston, D., et al. 2002, ApJ, 571, L85

Mellier, Y. 1999, ARA&A, 37, 127

Prada, F., Vitvitska, M., Klypin, A., et al. 2003, ApJ, 598, 260

Schirmer, M., Erben, T., Schneider, P., et al. 2003, A&A, 407, 869

Schneider, P., & Rix, H. 1997, ApJ, 474, 25

Sheldon, E. S., Johnston, D. E., Frieman, J. A., et al. 2004, AJ, 127, 2544

Smith, D. R., Bernstein, G. M., Fischer, P., & Jarvis, M. 2001, ApJ, 551, 643

Taylor, A. N., Bacon, D. J., Gray, M. E., et al. 2004, MNRAS, 353, 1176

Wilson, G., Kaiser, N., Luppino, G. A., & Cowie, L. L. 2001, ApJ, 555, 572

Wolf, C., Meisenheimer, K., Kleinheinrich, M., et al. 2004, A&A, 421, 913

Wolf, C., Meisenheimer, K., Rix, H.-W., et al. 2003, A&A, 401, 73